P10.1

POLARIMETRIC CHARACTERISTICS OF TORNADIC AND NONTORNADIC SUPERCELL THUNDERSTORMS

Matthew Kumjian* and Alexander Ryzhkov
Cooperative Institute for Mesoscale Meteorological Studies, University of Oklahoma, Norman, Oklahoma

1. INTRODUCTION

Polarimetric radar offers remarkable insight into the microphysics of severe convective storms that may be used to elucidate processes associated with tornadogenesis. Fourteen supercell thunderstorms have been observed by the research polarimetric WSR-88D S-band radar in Norman, Oklahoma (KOUN). Additionally, severe storm data from the EEC Sidpol C-band dual-polarization radar in Enterprise, Alabama and from the King City C-band dual-polarization radar in Ontario, Canada are presented. This study analyzes data from throughout the lifetime of fifteen supercell thunderstorms, nine of which were tornadic (including one from Alabama) and six that were nontornadic, as well as three nonsupercell storms, two of which were tornadic. The dates and times of the analyzed storms are shown in Table 1. The polarimetric radar variables that were utilized include radar reflectivity factor at a horizontal polarization (Z_{HH}; hereafter reflectivity), differential reflectivity (Z_{DR}), co-polar cross-correlation coefficient (ρ_{hv}), and specific differential phase (K_{DP}). For a review of the polarimetric variables, see Zrnić and Ryzhkov (1999).

A number of repetitive polarimetric signatures are found in these storms. These features include the tornadic debris signature associated with tornado touchdown, hail signatures reaching the ground, a Z_{DR} "arc" at low levels, reduced ρ_{hv} in the storm inflow region at low levels, Z_{DR} and K_{DP} columns extending above the melting layer, and midlevel "rings" of enhanced Z_{DR} and decreased ρ_{hv}. The locations of these features are shown in conceptual plan-position indicators (PPIs) in Figure 1. It should be noted that the tornado debris signature (TDS) is only present in the tornadic supercells.

Each of the aforementioned signatures will be described in more detail in the following section. Section 3 will focus on one of these signatures, the Z_{DR} arc. To investigate the Z_{DR} arc, a numerical model is developed and described in subsection 3.1. The results from this model are presented in subsection 3.2, followed by a discussion in section 4. A brief summary and conclusions are presented in section 5.

* *Corresponding author address:* Matthew R. Kumjian, National Weather Center, 120 David L. Boren Blvd., Room 5426, Norman, OK 73072; email: matthew.kumjian@noaa.gov

Date	T/N	Time of Observation (UTC)
8 May 2003	T	2145 – 2329
7 – 8 May 2003	N	0358 – 0555
10 May 2003	T	0120 – 0457
19 – 20 May 2003	N	2303 – 0107
26 - 27 May 2004	N	2236 – 2438
29-30 May 2004	T	2159 – 0630
10 November 2004	T	2208 – 2418
10 – 11 April 2005a	T	2247 - 0207
10 – 11 April 2005b	N	0039 - 0207
19 August 2005+	T	1740
13 September 2005	N	0044 – 0209
15 November 2006*	N	1803
1 March 2007*	T	1908
29 March 2007	T	2047 – 2125
10 April 2007	N	2257 – 0053
7 May 2007	T	0201 – 0247
8 May 2007	T	0002 – 0126
9 May 2007	T	0358 – 0502

*Table 1: Storm cases analyzed in this study. The date and time (in UTC) are given, along with whether the supercell was tornadic (T) or nontornadic (N). The asterisk (*) indicates that the data come from the Sidpol C-band polarimetric radar in Enterprise, Alabama, and the cross (+) indicates data from the King City C-band polarimetric radar in Ontario, Canada. All other cases are from the S-band KOUN in Norman, OK.*

2. POLARIMETRIC SIGNATURES

2.1 *Tornadic Debris Signature*

Ryzhkov et al. (2002) first noted a polarimetric signature at the tip of the hook echo in a supercell associated with lofted tornadic debris. Subsequent studies have shown that the tornadic debris signature (TDS) is found consistently at S band and that it could be used for tornado detection (Ryzhkov et al. 2005). Additionally, the TDS has been documented at C band (Conway et al. 2007) and X band (Bluestein et al. 2007). The signature is present when tornadoes loft debris since the random orientation, irregular shape, and high refractive index of debris results in high Z_{HH}, low Z_{DR}, and anomalously low ρ_{hv}. Typically, the signature is observable at relatively close ranges and for strong

tornadoes (EF-2 or stronger); at large distances, the radar resolution volume is large enough that it may smear out the signature. An example of the TDS is shown in Figure 2.

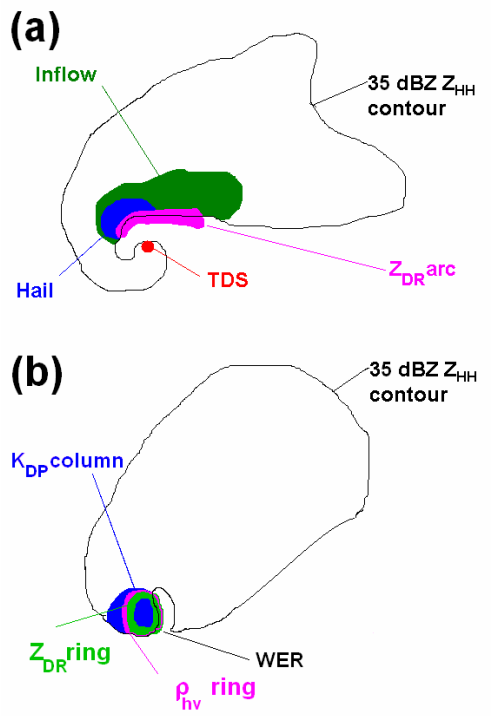

Fig. 1: (a) Low-level and (b) midlevel schematics of supercell thunderstorms with the locations of the polarimetric signatures indicated. "TDS" is the tornadic debris signature; "hail" is the low-level signature of hail reaching the ground; "inflow" is the low-level inflow signature; "WER" is the weak echo region.

2.2 *Hail Signature in the Forward-Flank Downdraft*

Hail is present in virtually every supercell due to the severe nature of such storms. Because hailstones tumble when they fall (Lesins and List 1986), they appear spherical in a statistical sense. This combined with the lower dielectric constant of ice (compared to water) results in low or near-zero values of Z_{DR}. Because of their large size, Z_{HH} is often high. Thus, high Z_{HH} and low Z_{DR} at the lowest tilt are good indicators of hail reaching the ground. The most common location for this signature is typically just to the north or northwest of the mesocyclone (low-level Z_{HH} hook) in the forward flank downdraft (FFD), as shown schematically in Figure 1. ρ_{hv} can also be reduced in the case of rain mixed with hail. An example of an observed hail signature is shown in Figure 3. For a recent review and more examples of polarimetric hail detection and verification, see Heinselman and Ryzhkov (2006).

2.3. *Low-level Inflow Signature*

Near-surface inflow into supercells can be intense (exceeding 25 m s^{-1}). Because of these strong winds, insects and/or other light debris including grass, leaves, dust, etc. can be ingested into the storm updraft. This debris is nonmeteorological and thus is characterized by low ρ_{hv}. The low-level inflow region along the forward-flank downdraft (FFD) and reflectivity hook may then have a mixture of precipitation particles and non-meteorological targets, subsequently reducing the ρ_{hv}.

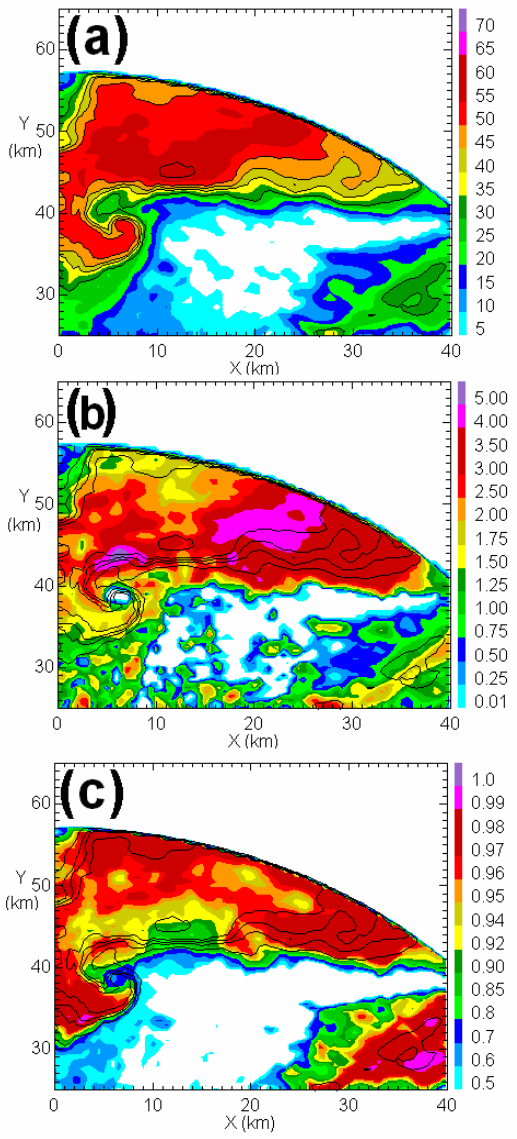

Fig. 2 Polarimetric tornadic debris signatures in three polarimetric radar variables: (a) Reflectivity factor (Z_{HH}); (b) Differential reflectivity (Z_{DR}); (c) Cross-correlation coefficient (ρ_{hv}) from 10 May, 2003 at 0346 UTC, shown on a 0.50 km constant-altitude PPI. Contours of Z_{HH} are overlaid on each of the panels to provide reference.

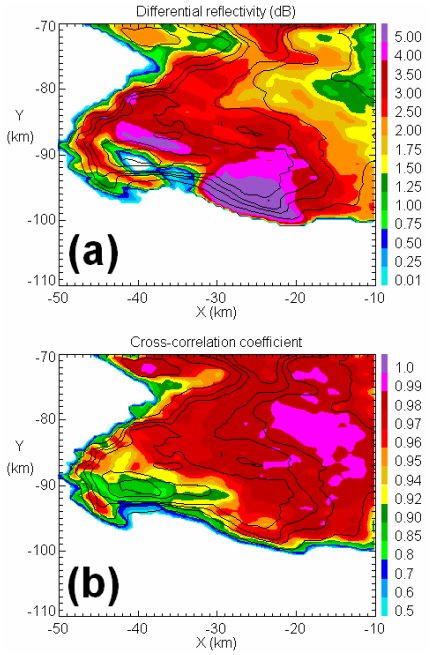

Fig. 3 Polarimetric signature of hail reaching the ground as shown in this 0.00km CAPPI from 19 May, 2003 at 2355 UTC. Polarimetric radar variables shown are (a) Z_{DR} and (b) ρ_{hv}. Contours of Z_{HH} are overlaid.

Figure 4 shows an example from the May 30, 2004 tornadic supercell in which television news cameras showed light debris from a recently plowed field being ingested into the storm (Schuur 2006, personal communication). This signature is widespread and usually relatively weak and should not be confused with the very localized and prominent tornado debris signature. The ingestion of light debris into the main updraft is evident by decreased ρ_{hv} aloft collocated with the updraft. The decreased ρ_{hv} aloft can also be due to lack of hydrometeors (low signal to noise ratio, Ryzhkov et al. 2002), or tumbling hailstones within the updraft core. Thus, in the absence of a clearly-defined bounded weak echo region (BWER), the area of decreased ρ_{hv} may be used as a proxy for the updraft location. Additionally, Ryzhkov et al. (2005) speculates that the decrease in ρ_{hv} may be an indirect measure of updraft strength.

2.4. Z_{DR} Arc Signature

Perhaps the most striking low-level feature observed in all supercell thunderstorms is the Z_{DR} arc signature, which occurs on the right (usually the southern) edge of the FFD, as shown in the schematic in Figure 1. The signature is not collocated with the Z_{HH} maximum; instead, it is usually found along the gradient in reflectivity. Z_{DR} values in excess of 4 – 5 dB are not uncommon at S band and may be even more prominent at C band. Examples from several storms in different climate regions are shown later in Figures 9, 10, 12, and

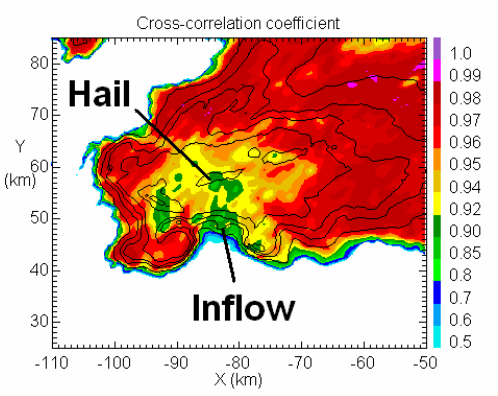

Fig. 4: 0.00km CAPPI showing the reduced ρ_{hv} as a result of light debris being ingested into the storm and hail at low levels. From 30 May, 2004 at 0023 UTC. Contours of Z_{HH} are overlaid.

13. This signature will be described in detail in section 3.

2.5. Z_{DR} and K_{DP} Columns

The prominence of Z_{DR} and K_{DP} columns associated with severe thunderstorm updrafts has made them some of the most frequently reported polarimetric signatures of convective storms (e.g., Caylor and Illingsworth 1987; Conway and Zrnić 1993; Tuttle 1993; Brandes et al. 1995 to name a few). Both tornadic and nontornadic supercell thunderstorms have very intense updrafts and thus have quite prominent columns. The columns typically extend several kilometers above the environmental melting layer and are indicative of a positive temperature perturbation associated with the updraft core. Supercooled liquid water drops and water-coated hailstones and graupel are most likely the cause of such columns. Brandes et al. (1995), and Loney et al. (2002) have in-situ measurements from these columns in severe hailstorms and offer a thorough description of the microphysics of each particular storm. The columns tend to be slightly offset during the mature mesocyclone phase of the supercell, with the K_{DP} column located slightly to the west (upshear) of the Z_{DR} column.

An example RHI through a particularly prominent Z_{DR} column is shown in Figure 5. The large positive values (> 2 dB) extend to about 7 km, which is well above the environment freezing level. Also note that the Z_{DR} column is located on the downwind periphery of the BWER, which marks the main updraft. The supercell updraft (BWER) is so intense that all hydrometeors are lofted and unable to fall. At the periphery of the main updraft core where the intensity of the vertical velocity is diminished the largest raindrops and coated hailstones begin to fall, enhancing the Z_{DR}. In Figure 5, the very low Z_{DR} centered on 39.5 km that extends about 2 km in height is the tornado debris column (see section 2.1).

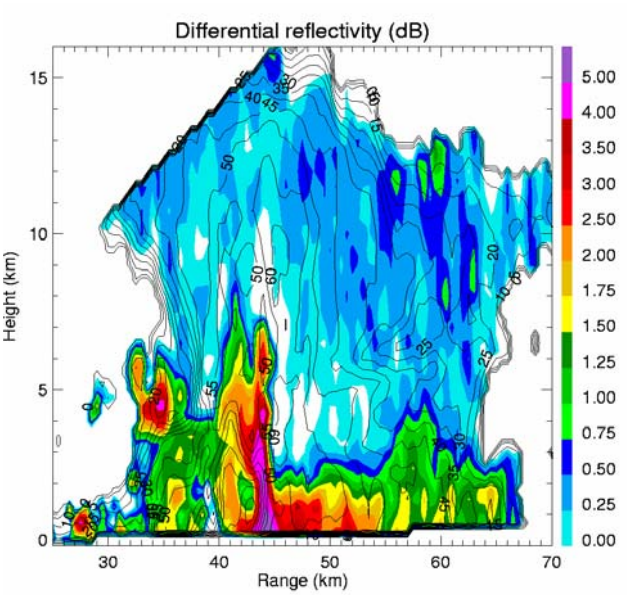

Fig. 5: A particularly prominent Z_{DR} column displayed at a range of about 44 km in this RHI through the 10 May, 2003 supercell at 0346 UTC through the 10° azimuth. High positive values of Z_{DR} (> 2 dB) extend up to about 7 km. Also note the tornado debris signature at a range of 39.5 km. Contours of Z_{HH} are overlaid.

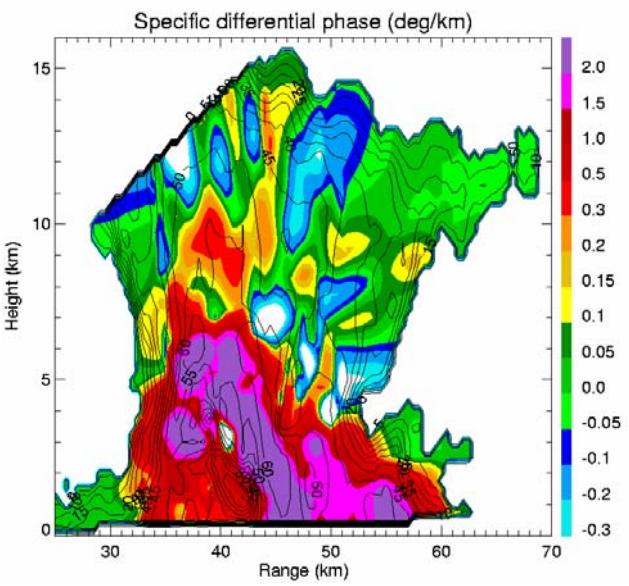

Fig. 6: A K_{DP} column displayed at a range of about 46 km in this RHI through the 10 May, 2003 supercell at 0340 UTC along the 2° azimuth. High positive values of K_{DP} (> 2 deg km^{-1}) extend up to about 6.5 km. Contours of Z_{HH} are overlaid.

A strong K_{DP} column from the 10 May, 2003 supercell is shown in the RHI in Figure 6, centered on a range of 46 km. The large positive values (>2 deg km^{-1}) extend to a height of about 6.5 km. The column is clearly separated spatially from the BWER. Taking the difference in azimuth angle into consideration, it is important to note that the K_{DP} column here is located to the north and west of the BWER and thus upshear of the Z_{DR} column.

2.6. *Midlevel Z_{DR} and ρ_{hv} Rings*

In both tornadic and nontornadic supercell thunderstorms a midlevel semi-circular or circular ring of enhanced Z_{DR} and depressed ρ_{hv} is sometimes found above the environmental melting layer and most likely near the updraft-perturbed melting layer, which can be crudely estimated using parcel theory. For the spring cases, the perturbed melting layer is typically around 5 km. The signatures are not always present throughout the lifetime of the storm, but when they appear they can be striking (Figs. 7 and 8 show several examples).

It is evident in Figure 7 that the southern side of the Z_{DR} ring is characterized by typically higher values. This is most likely due to renewed updraft growth on this flank, which is characteristic of right-moving supercell storms (Davies-Jones 1984; Brandes et al. 1988; Davies-Jones 2004). Additionally, the Z_{DR} ring is sometimes only a half ring (Fig. 7d); in this case it is always on the eastern or right flank of the updraft. A midlevel downdraft or entrainment could be the reason for the lack of a ring on the western flank. Figure 8 shows several examples of the midlevel rings of depressed ρ_{hv}. Similar to the Z_{DR} rings, the shape may or may not be a full circular ring; again it is preferentially on the eastern or right flank of the updraft.

The circular or semi-circular appearance of the Z_{DR} and ρ_{hv} rings and their relative location to the updraft and mesocyclone provide strong evidence that they are associated with cyclonic vorticity. The fact that the rings are generally spatially offset from one another hints at an analog to the standard melting layer signature (for more information on polarimetric melting layer signatures and detection, see Ryzhkov and Zrnić 1998; Giangrande and Ryzhkov 2004; Giangrande et al. 2005). The significance of the shape (i.e., being a full ring versus a half ring) and the analog to a melting layer signature are speculative; future work will investigate this signature in more detail. Another possible explanation is that the relatively sparse concentration of large drops on the periphery of the updraft associated with the Z_{DR} column is wrapped around by the mesocyclone. This would also result in enhanced Z_{DR} values and decreased ρ_{hv}. Trajectory analyses must be completed to determine which (if any) of these hypotheses is true.

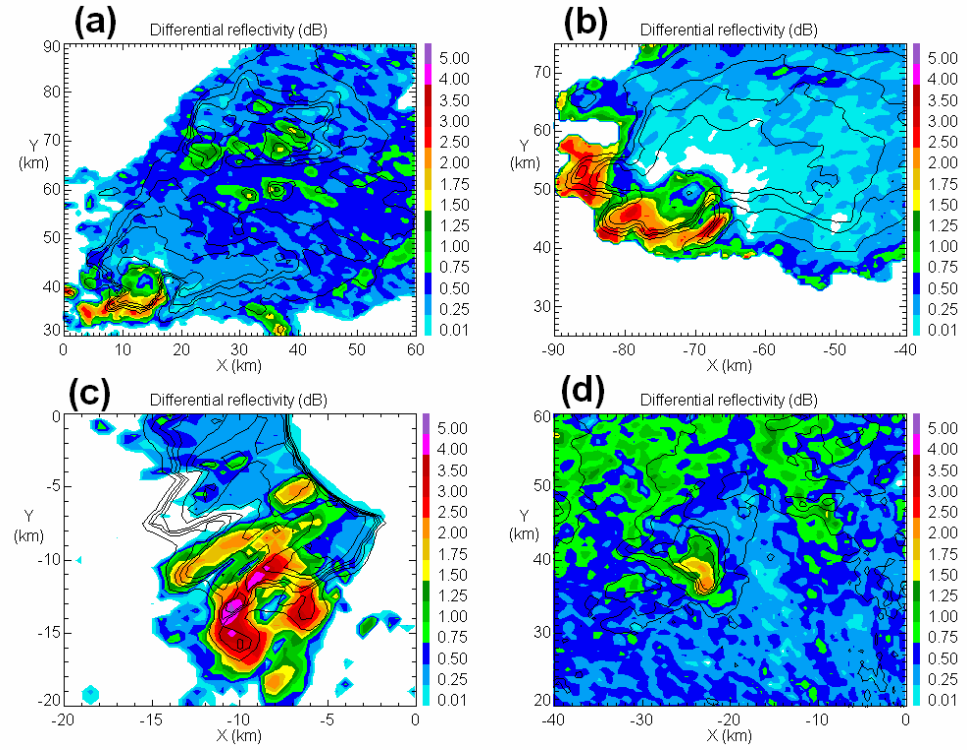

Fig. 7: Four examples of Z_{DR} rings at midlevels of the storms: (a) 10 May, 2003, taken at 5.0 km at 0351 UTC; (b) 30 May, 2004, taken at 4.0 km at 0044 UTC; (c) 10 April, 2005, taken at 2.5 km, at 2354 UTC; (d) 29 March, 2007, taken at 4.0 km, at 2106 UTC. Contours of Z_{HH} are overlaid.

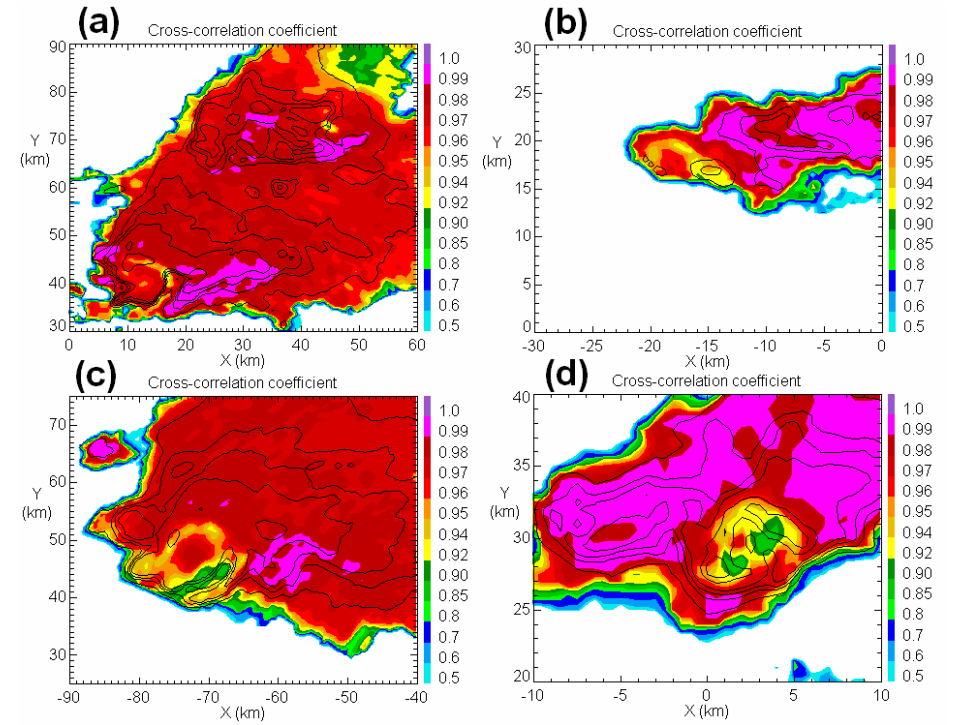

Fig. 8: Four examples of ρ_{hv} rings at midlevels of the storms: (a) 10 May, 2003, taken at 5.0 km at 0351 UTC; (b) 27 May, 2004, taken at 4.75 km at 0025 UTC; (c) 30 May, 2004, taken at 5.5 km, at 0044 UTC; (d) 10 November, 2005, taken at 2.5 km, at 2221 UTC. Contours of Z_{HH} are overlaid.

3. MORE ON THE Z_{DR} ARC SIGNATURE

The utility of integrating polarimetric data and conventional Doppler radar is readily shown by the wealth of information about the storm's microphysics evident through the polarimetric signatures described in this study so far. Hail and tornadoes have been studied extensively in supercell thunderstorms, but relatively little work has been done in the analysis of microphysics. This is partly due to the lack of observational capabilities, since flying aircraft into supercells can be extremely dangerous and conventional single-polarization radars are not adequate for microphysics studies. Dual-polarization radar, however, offers significant insight.

The remainder of this paper will focus on the Z_{DR} arc signature introduced in section 2.4. The Z_{DR} arc signature is a shallow feature, usually found below 2 km. It has been observed in different climate regions, including the Great Plains (Ryzhkov et al. 2005), Canada, and the southeastern United States at both S- and C-bands (Ryzhkov et al. 2005; Conway et al. 2007). Figure 9 shows examples of this signature from different supercell storms observed with KOUN (S-band), and Figure 10 shows C-band observations of the Z_{DR} arc from the 1 March 2007 tornadic supercell in Enterprise, Alabama.

The arc is always located in the same relative position of the storm along the Z_{HH} gradient on the southern (right) edge of the FFD. It is clear from Figures 9 – 10 that it can be more or less prominent depending on the case. The examples in Figure 9 show the arc at a variety of distances from the radar. However, if the supercell is so far from the radar that the beam of the lowest elevation angle scan is more than 1 – 2 km above the ground, the beam may overshoot the shallow signature. In contrast, the Enterprise storm (Fig. 10) was so close to the radar that the Z_{DR} arc is seen with extremely high detail. At higher elevation angles (not shown), the arc is clearly seen wrapping around the near-surface mesocyclone.

The Z_{DR} arc is found in both tornadic and nontornadic supercell storms throughout their mature lifetime. The ubiquitous nature of the signature in all supercells provides strong evidence that it is related to intrinsic microphysical and kinematic properties of these storms. We believe that the arc is caused by veering of the wind, a property of supercell environments. In the next subsection we will describe a numerical model created to investigate this hypothesis.

3.1. *The Model*

A very simple numerical model was constructed for this study. The domain is 5 km x 5 km in the horizontal and 3 km tall. Horizontal resolution is 500 m and vertical resolution is 200 m. At the top of the domain, a precipitating cloud is allowed to rain into the domain starting at time t = 0. The cloud itself is 3 km x 3 km and is initially in the bottom right corner of the domain. The initial DSD is prescribed as a Marshall-Palmer (1948) with rainfall rate R = 30 mm hr^{-1}. No coalescence, collisions, or other raindrop interactions are included. Additionally, evaporation and drop break-up are neglected.

Any vertical wind profile can be prescribed throughout the domain and is assumed to be horizontally homogeneous. No environmental vertical velocities are included. To make the flow storm-relative (and to keep the cloud within the domain), an assumed storm motion vector is subtracted off the wind profile. Hodographs for different experiments are shown with the resulting Z_{DR} distributions in the next subsection.

The cloud is subdivided into "parcels" 100 m x 100 m, each filled with a Marshall-Palmer distribution of raindrops. After the experiment begins, the drops of different sizes fall out and follow different trajectories. Each drop size is followed in a Lagrangian sense. Once an allotted amount of time has passed, a particular height of interest is chosen to investigate the distribution of polarimetric variables. The different-sized drops at this level are accounted for and the radar variables Z_{HH}, Z_{DR}, and K_{DP} are calculated. Plots are made such that the contours of Z_{HH} are overlaid on all three variables to get a sense if the resultant fields of Z_{DR} and K_{DP} are spatially offset, as in the observational data shown above. For the experiments in this study, the height chosen is 400 m. The simulations are allowed to run for Δt = 600 s.

3.2. *Model Results*

Numerous experiments were conducted to investigate the effect of different vertical wind profiles on the size-sorting mechanism that causes the Z_{DR} arc signature in supercell thunderstorms. For each of these experiments, the hodograph is plotted in the left panel and the resulting Z_{DR} field is plotted in the right panel in Figure 11. The thin red line is the environmental hodograph, the blue circle is the tip of the storm motion vector, and minus two times the light blue shading is the 0 – 3 km storm-relative environmental helicity (SREH). SREH is given by:

$$SREH = \int_0^{3\,km} \left(\vec{v}_H - \vec{c}\right) \cdot \nabla \times \vec{v}_H \, dz \tag{1}$$

where $\vec{v}_H$ is the horizontal environmental wind and $\vec{c}$ is the storm motion vector.

The first experiment is a control run with no wind (Fig. 11a), allowing the drops to fall freely through the domain. As expected, the resultant field of Z_{DR} (Fig. 11b) is uniform, and no arc signature is present. It is evident that the large drops do not dominate the DSD because the maximum Z_{DR} value is only 1.75 dB. In Figure 11c, an idealized 1/4-circle hodograph is used. The wind speed is a constant 10 m s^{-1} at each level but the direction veers uniformly from a southerly wind at the surface to a westerly wind at 3 km. The

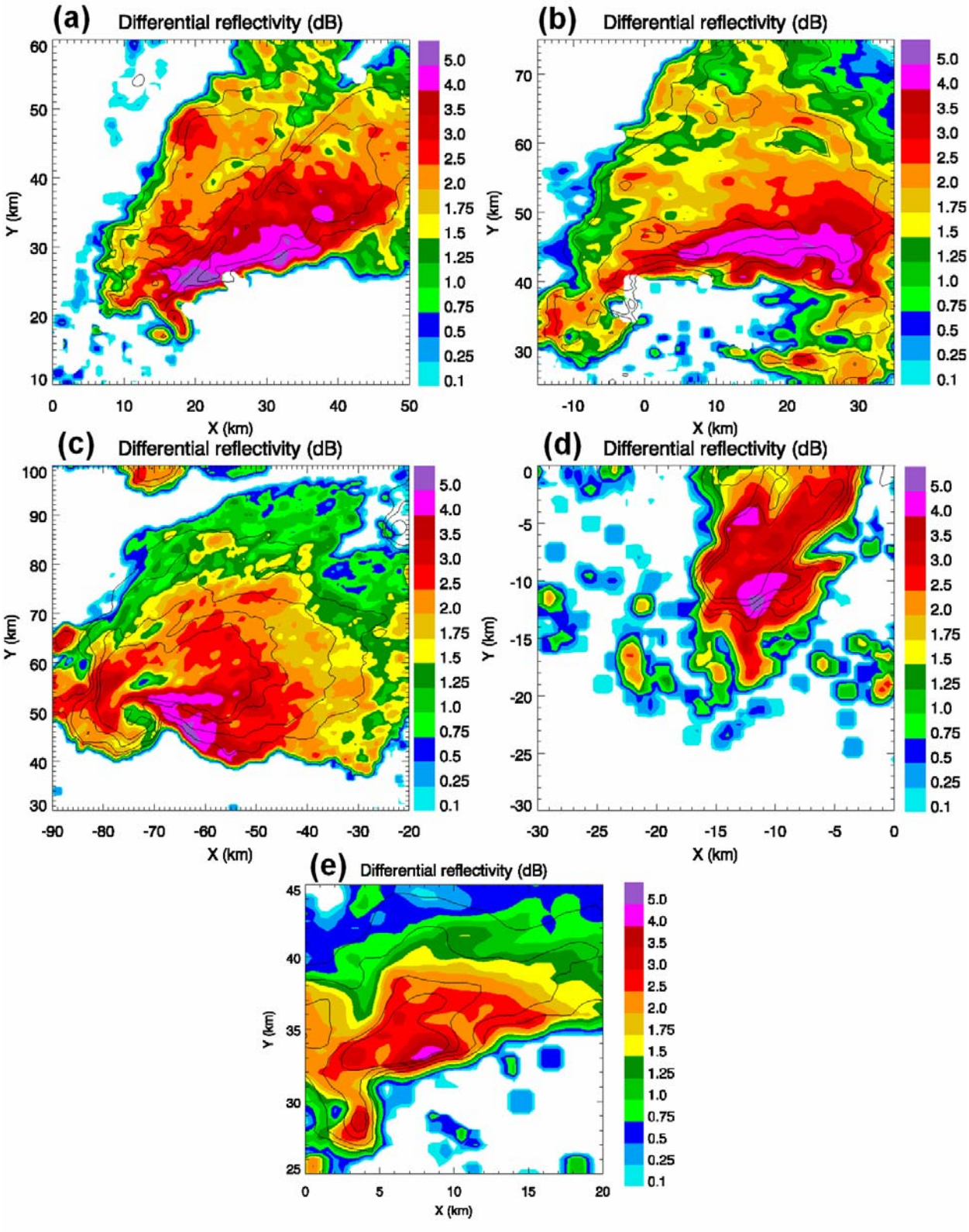

Fig. 9: Low-level PPI scans showing the Z_{DR} arc signature. (a) From 8 May, 2003 at 2234 UTC, 1.5°; (b) 10 May, 2003 at 0333 UTC, 0.5°; (c) 30 May, 2004 at 0044 UTC, 0.5°; (d) 10 April, 2005 at 2354 UTC, 1.5°; (e) 10 November, 2004 at 2228 UTC, 1.5°.

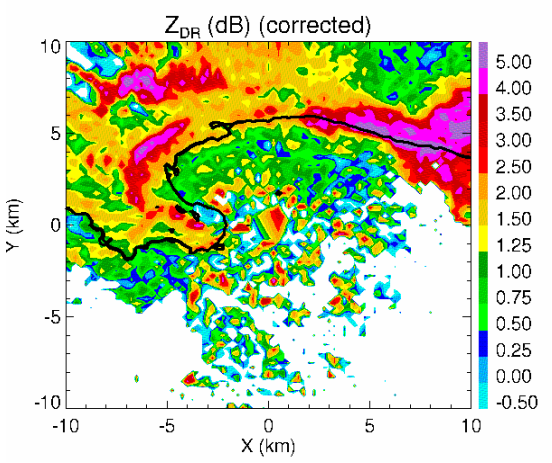

Fig. 10: Low-level (0.5°) PPI scan showing the Z_{DR} arc signature from the Enterprise Sidpol C-band polarimetric radar. Data is from the 1 March, 2007 1908 UTC devastating tornado. Note the extremely low Z_{DR} at the tip of the hook echo, indicative of tornadic debris.

storm motion is westerly at 10 m s^{-1}. In the resulting field of Z_{DR} (Fig. 11d) we see an enhancement of values along the southern edge of the Z_{HH} gradient, exactly what is observed in real supercells. Increasing the 1/4-circle hodograph to 15 m s^{-1} and the storm motion vector to 15 m s^{-1} (Fig. 11e) results in a quite striking Z_{DR} arc (Fig. 11f), with maximum values of about 4.5 dB.

A relationship between the SREH and the maximum Z_{DR} is evident when comparing the hodographs to the maximum Z_{DR} values. This simple model shows that increasing SREH leads to stronger Z_{DR} arc signatures. Thus, we may speculate that the strength of the Z_{DR} arc signature may be an indirect measure of the SREH for that particular storm. Since typical SREH values are estimated from 00 UTC and 12 UTC soundings at a given point, using an estimated or pre-calculated storm motion vector, the Z_{DR} arc may have significant operational value for forecasters in determining storm severity and potential for tornadoes.

4. DISCUSSION

The previous sections have shown the importance of size sorting in supercell thunderstorms in creating enhanced regions of Z_{DR}. Very high (>3 dB) values of Z_{DR} indicate an absence of smaller drops, creating a significantly modified or truncated drop size distribution (DSD). Mechanisms of size sorting are typically kinematic. Strong vertical shear (as described above) will produce differential drop trajectories. Smaller drops that fall with lower terminal velocities will be advected further downwind than larger drops that fall faster. Vertical velocities associated with convective updrafts will sort drops as well. Smaller drops are lofted by the updraft while larger drops can fall out, enhancing Z_{DR} below developing convective updrafts, resulting in a Z_{DR} column. In the case of strong rotation as in a tornado, larger particles are centrifuged further than smaller particles (Dowell et al. 2005).

In most existing storm-scale numerical models, size-sorting and explicit microphysics are not accounted for. Instead, computed quantities like liquid water mixing ratio along with an assumed DSD are used to calculate radar variables. The assimilation of dual-polarization data into storm-scale models will only benefit forecasts if the model is able to reproduce the observed polarimetric signatures. Unfortunately, this is virtually impossible for bulk-microphysics parameterization schemes. If the models cannot capture the polarimetric signatures described here, then they do not capture the intrinsic microphysics of supercell storms. The failure of existing models to capture the microphysics should be a warning flag for modelers.

The Z_{DR} arc is indicative of a kinematic property of supercell storms, so it is unique in that it can be seen through polarimetric observations of microphysical processes in the storm. It is important to emphasize that this is not just an azimuthal shear signature like a Doppler velocity couplet or tornado vortex signature (TVS); instead, the arc signature indicates a *vertical* shear. It is very difficult to view this type of veering from Doppler velocities, and it is fundamentally impossible to assess vertical shear profiles from the Doppler velocities of one elevation scan. In order to assess the vertical profile of winds in the storm, one must compare different tilts simultaneously, which in an operational setting is time-consuming. Additionally, with a veering profile, Doppler velocities will go to zero at some level since the true wind field will be perpendicular to the radar beam.

In nonsupercell thunderstorms, the signature may indicate the onset of vorticity generation due to strong SREH values, which can be thought of as a measure of how streamwise the environmental vorticity is that is being ingested into the storm (Davies-Jones 1984). In other words, a Z_{DR} arc appearing in a convective storm may indicate the onset of updraft rotation (a mesocyclone). Once midlevel vorticity is produced, other polarimetric signatures described in this paper such as the midlevel Z_{DR} ring may be used to confirm the onset of storm-scale rotation.

Strong veering of the wind (large values of SREH) is usually associated with severe weather. Many studies (e.g., Fawbush and Miller, 1954; Maddox, 1976; Darkow and McCann, 1977; Davies-Jones, 1984) have established the relationship between storm intensity and speed and directional shear of environmental winds. Thus, this Z_{DR} arc signature could be a measure of SREH, and more importantly an indicator of storm severity. Figures 12 and 13 show several examples of cases in which a Z_{DR} arc appears in nonsupercell convective storms in which damaging winds (in one case) and a tornado (in the others) resulted. In Figure 13, a weak Z_{DR} arc is present at 0422 UTC. Fourteen minutes later (0436 UTC), a midlevel Z_{DR} half-ring appeared (not shown). This is indicative of cyclonic vorticity at midlevels, which could mark the onset of

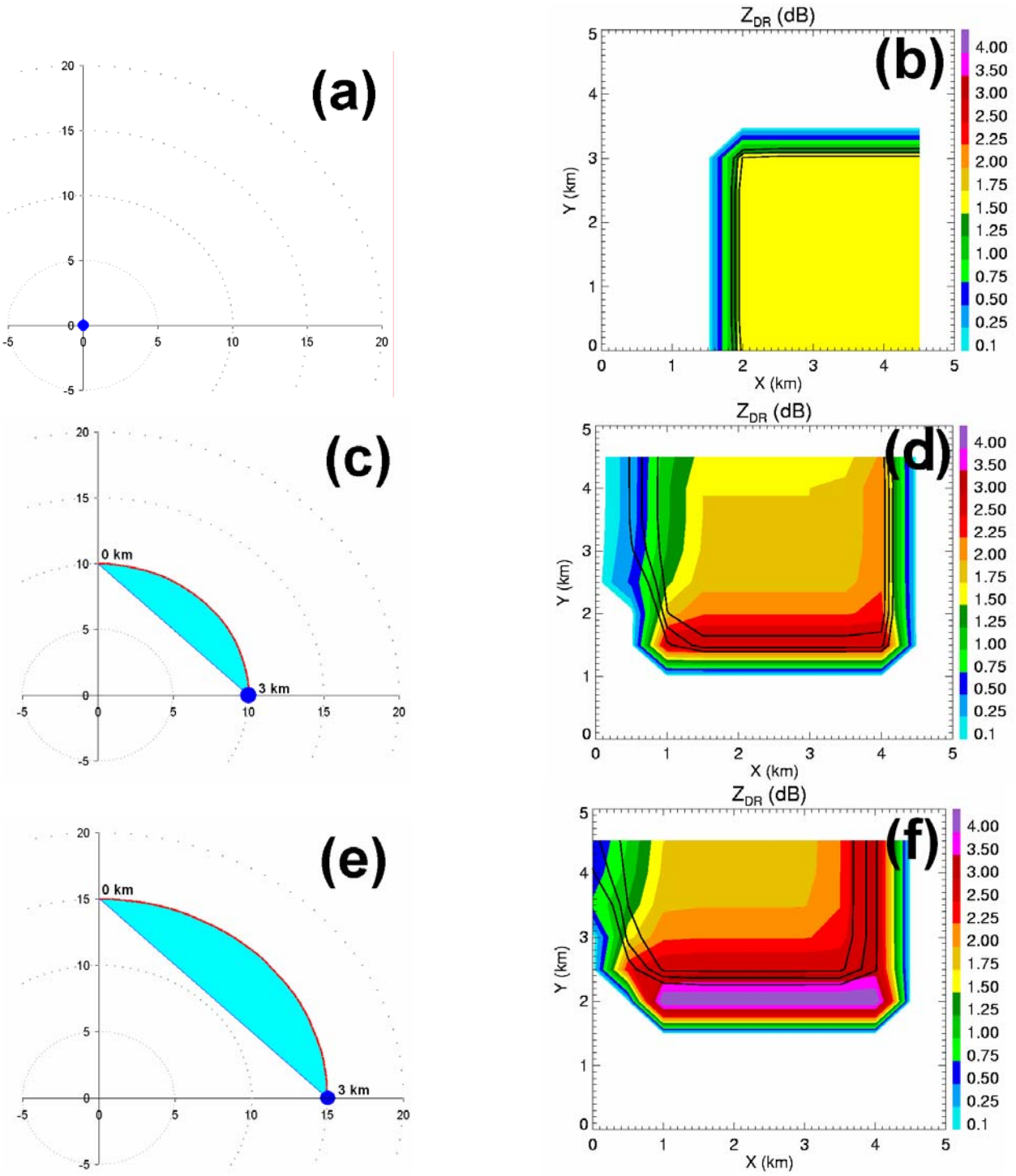

Fig. 11: Model results for various hodographs. Surface to 3 km hodographs are shown on the left. The red line is the environmental flow, the blue dot is the storm motion vector, and the light blue shading is proportional to the 0-3 km storm relative environmental helicity (SREH). The model results of Z_{DR} at 400 m are shown on the right, with contours of Z_{HH} (30 dBZ, 35 dBZ, and 40 dBZ) overlaid.

updraft rotation. Nine minutes after the midlevel Z_{DR} ring (0445 UTC), the storm produced a high-end EF-1 tornado.

Ordinary non-severe convective storms do not display such a signature, though they may display a locally enhanced Z_{DR} region associated with an updraft. The updraft Z_{DR} enhancement will be associated with a column (see section 2.5), whereas the Z_{DR} arc is a very shallow, elongated signature typically along the reflectivity gradient. Thus, it should be easy to distinguish between these two polarimetric features.

5. SUMMARY AND CONCLUSIONS

This study has pointed out several repetitive polarimetric signatures of tornadic and nontornadic supercell thunderstorms. Because these signatures are present in all supercells and are consistent throughout the mature lifetime of the storms, they are significant in that they may indirectly illuminate kinematic or microphysical properties that are intrinsic in supercells. Additionally, the signatures may provide insight into storm evolution and behavior for operational meteorologists. One signature in particular, the Z_{DR} arc, may indicate storm severity even in nonsupercell thunderstorms, as it is a manifestation of a vertical shear profile exhibited in the microphysics and is observable with polarimetric radar. Although no differences between tornadic and nontornadic supercells are presented in this study, future work and further scrutiny of the growing data set may offer more insight into processes associated with tornadogenesis.

6. ACKNOWLEDGEMENTS

The authors would like to thank the NSSL/CIMMS employees who maintain and operate the KOUN polarimetric radar. We are also grateful for the polarimetric data from Environment Canada and Weather Decision Technologies, Inc. Additionally, useful discussions with Gabe Garfield, Dr. Alan Shapiro, Scott Giangrande, Alex Schenkman, and others aided the completion of this study.

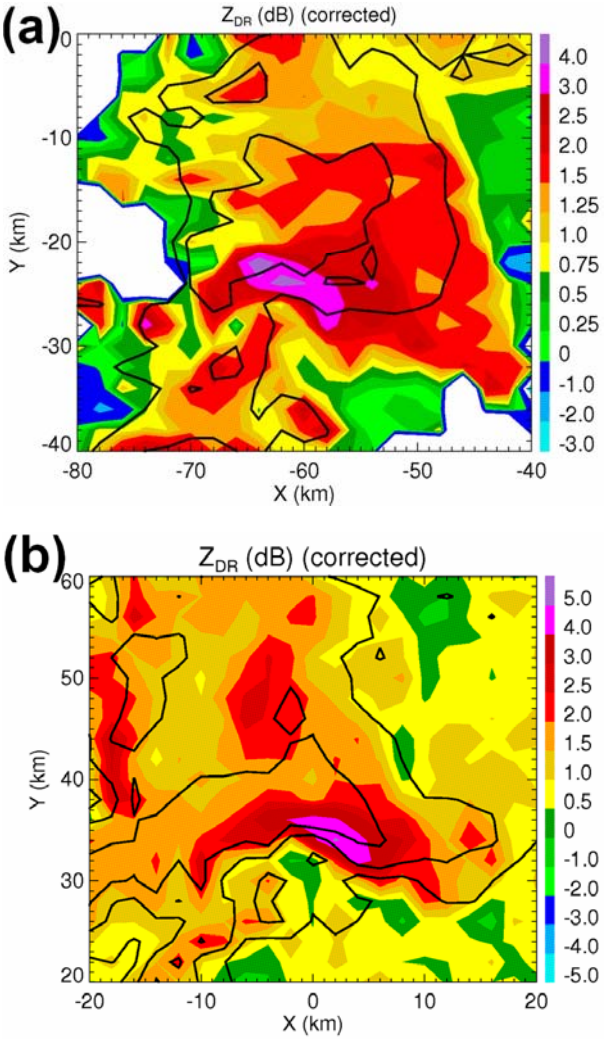

Fig. 12: Z_{DR} arc signature from convective cells embedded in a mesoscale convective system (MCS). (a) from 19 August 2005 at 1740 UTC, observed by the King City C-band polarimetric radar in Ontario, Canada. (b) from 15 November 2006 at 1803 UTC, as observed by the Sidpol C-band polarimetric radar in Alabama. Low-level (0.5°) PPIs shown; the storm in (a) produced a small tornado; the storm in (b) did not produce a tornado but did cause damaging winds. 30 dBZ, 40 dBZ, and 50 dBZ contours of Z_{HH} are overlaid.

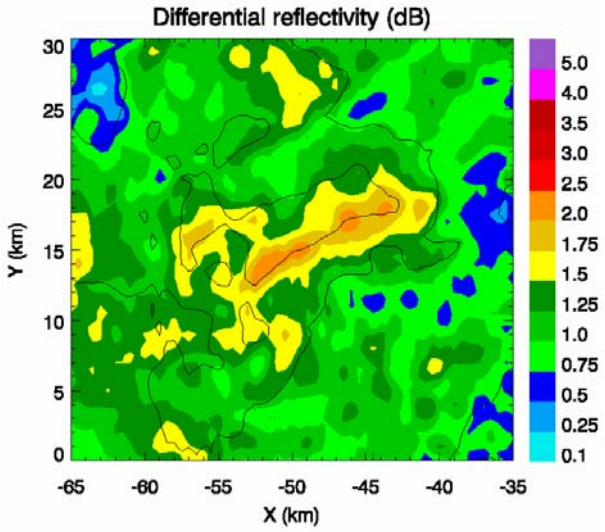

Fig. 13: A weaker Z_{DR} arc signature from a convective cell associated with a mesoscale convective vortex (MCV). Observed by KOUN polarimetric radar on 9 May, 2007 at 0422 UTC at an elevation of 0.9°. At 0436 UTC, a midlevel Z_{DR} half-ring appeared, indicative of cyclonic vorticity/updraft rotation. At 0445 UTC, the storm produced a high-end EF-1 tornado. 40 dBZ, 45 dBZ, and 50 dBZ contours of Z_{HH} are overlaid.

7. REFERENCES

Bluestein, H.B., M.M. French, R.L. Tanamachi, S.F. Frasier, K. Hardwick, F. Junyent, and A. Pazmany, 2007: Close-range observations of tornadoes in supercells made with a dual-polarization, X-band, mobile Doppler radar. *Mon. Wea. Rev.*, **135**, 1522-1543.

Brandes, E.A., R. Davies-Jones, B.C. Johnson, 1988: Streamwise vorticity effects on supercell morphology and persistence. *J. Atmos. Sci.,* **45**, 947-963.

———, J. Vivekanandan, J.D. Tuttle, and C.J. Kessinger, 1995: A study of thunderstorm microphysics with multiparameter radar and aircraft observations. *Mon. Wea. Rev.*, **123**, 3129-3143.

Caylor, I.J. and A.J. Illingsworth, 1987: Radar observations and modeling of warm rain initiation. *Quart. J. Roy. Meteor. Soc.*, **113**, 1171-1191.

Conway, J.W. and D.S. Zrnić, 1993: A study of embryo production and hail growth using dual-Doppler and multiparameter radars. *Mon. Wea. Rev.*, **121**, 2511-2528.

———, A. V. Ryzhkov, E. D. Mitchell, P. Zhang, L. Venkatramani, J. L. Alford, and D. Nelson, 2007: Examination of tornadic signatures observed at very close range using simultaneous dual-polarization radar at C band. Preprints, *33rd Int. Conf. on Radar Meteorology,* Cairns, Australia, Amer. Meteor. Soc., CD-ROM, P10.2.

Darkow, G.L. and D.W. McCann, 1977: Relative environmental winds for 121 tornado bearing storms. Preprints, *10th Conf. Severe Local Storms*, Omaha, NE, Amer. Meteor. Soc., 413-417.

Davies-Jones, R., 1984: Streamwise vorticity: The origin of updraft rotation in supercell storms. *J. Atmos. Sci.*, **41**, 2991-3006.

Davies-Jones, R., 2004: Growth of circulation around supercell updrafts. *J. Atmos. Sci.,* **61**, 2863-2876.

Dowell, D.C., C.R. Alexander, J.M. Wurman, and L.J. Wicker, 2005: Centrifuging of hydrometeors and debris in tornadoes: Radar-reflectivity patterns and wind measurement errors. *Mon. Wea. Rev.*, **133**, 1501-1524.

Fawbush, E.J. and R.C. Miller, 1954: The types of airmasses in which North American tornadoes form. *Bull. Amer. Meteor. Soc.*, **35,** 154-165.

Giangrande, S. E., and A. V. Ryzhkov, 2004: Polarimetric method for bright band detection. Preprints, 11th Conf. on Aviation, Range, and Aerospace Meteor., Hyannis, MA, Amer. Meteor. Soc., CD-ROM, P5.8.

———, ———, and J. Krause, 2005: Automatic detection of the melting layer with a polarimetric prototype of the WSR-88D radar. Preprints, *32nd Int. Conf. on Radar Meteorology*, Albuquerque, NM, USA, Amer. Meteor. Soc., CD-ROM, 11R.2.

Heinselman, P.L. and A.V. Ryzhkov, 2006: Validation of polarimetric hail detection. *Wea. Forecasting,* **21**, 839-850.

Kennedy, P.C., S.A. Rutledge, and W.A. Petersen, 2001: Polarimetric radar observations of hail formation. *J. Appl. Meteor.*, **40**, 1347-1366.

Lesins, G.B. and R. List, 1986: Sponginess and drop shedding of gyrating hailstones in a pressure-controlled icing wind tunnel. *J. Atmos. Sci.*, **43**, 2813-2825.

Loney, M.L., D.S. Zrnić, J.M. Straka, and A.V. Ryzhkov, 2002: Enhanced polarimetric radar signatures above the melting level in a supercell storm. *J. Appl. Meteor.*, **41**, 1179-1194.

Maddox, R.A., 1976: An evaluation of tornado proximity wind and stability data. *Mon. Wea. Rev.*, **104**, 133-142.

Marshall, J.S. and W. Palmer, 1948: The distribution of raindrops with size. *J. Meteor.*, **5**, 165-166.

Ryzhkov, A.V. and D.S. Zrnić, 1998: Discrimination between rain and snow with a polarimetric radar. *J. Appl. Meteor.*, **37**, 1228-1240.

———, D. Burgess, D.S. Zrnić, T. Smith, S. Giangrande, 2002: Polarimetric Analysis of a 3 May 1999 Tornado. Preprints, *21st Conf. on Severe Local Storms,* San Antonio, TX, Amer. Meteor. Soc., 515-518.

———, T.J. Schuur, and D.W. Burgess, 2005: Polarimetric tornado detection. *J. Appl. Meteor.* **44**, 557-570.

Tuttle, J.D., 1993: Multiparameter radar observations of developing turrets in a High Plains storm. Preprints, *26th Int. Conf. on Radar Meteorology*, Norman, OK, Amer. Meteor. Soc., 516-518.

Zrnić, D.S. and A.V. Ryzhkov, 1999: Polarimetry for Weather Surveillance Radars. *Bull. Amer. Meteor. Soc.* **80**, 389-406.